Electronic spectroscopy of UO2(2+), NUO(+) and NUN: an evaluation of time-dependent density functional theory for actinides.

Pawel Tecmer, Andre Severo Pereira Gomes, Ulf Ekström, Lucas Visscher

Electronic spectroscopy of UO_2^{2+}, NUO^+ and NUN: An Evaluation of Time-Dependent Density Functional Theory for actinides

Paweł Tecmer[a], André Severo Pereira Gomes[b], Ulf Ekström[a] and Lucas Visscher[a*]

Received Xth XXXXXXXXXX 20XX, Accepted Xth XXXXXXXXX 20XX
First published on the web Xth XXXXXXXXXX 200X
DOI: 10.1039/b000000x

The performance of the time-dependent density functional theory (TDDFT) approach has been evaluated for the electronic spectrum of the UO_2^{2+}, NUO^+ and NUN molecules. Different exchange-correlation functionals (LDA, PBE, BLYP, B3LYP, PBE0, M06, M06-L, M06-2X, CAM-B3LYP) and the SAOP model potential have been investigated, as has the relative importance of the adiabatic local density approximation (ALDA) to the exchange-correlation kernel. The vertical excitation energies have been compared with reference data obtained using accurate wave-function theory (WFT) methods.

last compilation: January 29, 2011

1 Introduction

The importance of theoretical modeling in furthering the understanding of the chemistry of actinide-containing systems, compared to other branches of chemistry, is by now well established. This prominent role has to do with the experimental difficulties involved in actinide research: besides the acute radiotoxicity of most species, which place severe restrictions on laboratory manipulations, the wide range of oxidation states possible for early actinides (U–Am), together with a relative ease of changing their oxidation states often makes it difficult to isolate and characterize species.

One of the most active areas of chemical research on actinides is related to the reprocessing of nuclear waste, whose objective is to separate uranium and plutonium from the other (minor) actinides. Such separation has implications both to the recycling of irradiated nuclear fuels (by allowing the retrieval of important quantities of U and Pu from spent fuel and their subsequent reconversion back to usable fuel) and to the disposal of nuclear waste (as it decreases the volume of material to be stored). While separation methods based upon liquid-liquid extraction ion-exchange, such as the plutonium uranium extraction (PUREX)[1,2] or transuranic extraction (TRUEX)[3] processes are rather well established, the details of the interaction of the extraction ligand with the actinide species (such as the simple atomic ions Ac^{n+} or the frequently found actinyl (AcO_2^{n+}) species) are still far from fully understood.

Bridging this gap in understanding would be particularly helpful in designing more efficient and selective complexing agents. Modeling this process is challenging, because it requires an accurate description of the actinide and the complexing species, as well as their interactions with the solvent environment. This is currently only possible with Density-Functional Theory (DFT), as its relatively modest computational cost makes the study of structure and energetics of relatively large model complexes possible, even in the condensed phase.[4–12]

Notwithstanding this progress, the success of DFT still depends on careful parametrization and benchmarking studies that establish the reliability of exchange-correlation functionals for a particular application. This is particularly serious for molecules containing heavy elements since such systems were usually not accounted for in the parametrization and validation stage of the currently available density functionals. One particular reason for concern is the strong (static and dynamic) electron correlation effects in actinides. The $5f, 7s, 6p$ and $6d$ orbitals should all be considered valence orbitals that can contribute to the chemical bonding. While energetically close, these orbitals have a rather different spatial character making the description of the exchange-correlation interaction by a density functional more difficult than for lighter elements. These difficulties have been investigated for uranium oxides[13], showing that DFT, using proper functionals, is typically suitable for geometry optimization and thermochemistry of the electronic ground state for these systems. Based on a series of studies of solvated uranium fluorides and oxofluorides

[a] *Amsterdam Center for Multiscale Modeling, Department of Theoretical Chemistry, Faculty of Sciences, Vrije Universiteit Amsterdam, De Boelelaan 1083, 1081 HV Amsterdam, Netherlands. E-mail: visscher@few.vu.nl*
[b] *Université de Lille 1 (Sciences et Technologies), Laboratoire PhLAM, CNRS UMR 8523, CNRS FR 2416, Bât P5, F-59655 Villeneuve d'Ascq Cedex, France*

Schreckenbach and Shamov [14] conclude that GGA functionals yield accurate geometries and frequencies while hybrid density functional theory (DFT) functionals are found to be superior for the thermochemistry.

The question of suitability of DFT for studying actinide-containing molecules carries over to its time-dependent generalization (TDDFT), which is is used to calculate properties depending upon the response of the density to an external perturbation. These calculations allow one to predict and analyze electronic spectra, polarizabilities or magnetizabilities, and vibrational Raman spectra, all of which are useful tools in studying the interactions of the actinide system with the complexing agents, or of that complex with the environment. While TDDFT has been shown to work rather well for some transition metal excited states [15–17], currently there are still only relatively few studies [18–20] assessing the reliability of TDDFT for actinide-containing molecules.

The aim of this paper is, therefore, to explore different flavors of TDDFT for the calculation of electronic spectra for such systems - that is, evaluating (meta-)GGAs and (meta-)hybrid functionals within the adiabatic approximation. We will also study the further approximation of replacing the derivatives of the functionals in the exchange-correlation (XC) kernel by the simpler LDA approach (ALDA) that is often used to simplify the implementation of TDDFT.

Our initial focus will be on small molecules, namely UO_2^{2+}, NUO^+ and NUN, since: (a) they are closed-shell systems in their ground-states, thus avoiding problems with the validity of the reference state for TDDFT; (b) they are all isoelectronic, making it instructive to see how changes in, for instance, electronegativity of the ligands affect the spectra; (c) the -N=U=N- and O=U=N- groups appear in larger organometallic systems, so they can serve as stepping stones for description of their oxo(MO), imido (MNR) and phoshorane iminato ($MNPR_3$) [21–24] analogs, which are very important in nuclear waste separation, and (d) in contrast to UO_2^{2+}, which has received extensive attention from theoreticians [18,20,25–30], the electronic spectra of the isoelectronic species NUO^+ and NUN [31–33]) have not yet been investigated in detail.

The lack of of experimental data requires that our assessment be done by comparison with accurate wavefunction-based (WFT) calculations, namely the complete active space second-order perturbation theory (CASPT2) [34,35] and intermediate Hamiltonian Fock-space coupled cluster (IHFSCC) [36–38] methods. Our aim in using both in tandem is to provide a cross-validation of WFT results, and to get access to the rich set of analysis tools available for CASPT2 (in our case population analysis of the excited states).

CASPT2 and IHFSCC are examples of multi-reference approaches to the electron correlation problem, and are know to perform well for actinide and other heavy element-containing molecules since such systems often present (nearly-)degenerate electronic states [19,39–41] (e.g. half-filled f shells etc). Unsurprisingly, they also show a very good performance in cases where the reference wavefunction is still dominated by a single determinant [27,42].

The IHFSCC method is particularly interesting here because of its ability to yield a number of electronic states of the molecule (and those due to electron attachment or detachment) in a single calculation. Furthermore, as all states have a common Fermi vaccum, it has as advantage the elimination of a potential bias towards a given reference state. The Intermediate Hamiltonian ansatz thereby circumvents a well-known drawback of the Fock Space (FS) (and other multireference coupled cluster) approaches by largely eliminating the intruder states that could otherwise obstruct the convergence of the FSCC algorithm. As it is beyond the scope of this work to discuss in depth IHFSCC and other coupled-cluster approaches for the calculation of electronic spectra, we refer the reader to recent reviews [43–45].

We note that spin-obit (SO) effects are small in the ground states of these molecules, with scalar relativistic and 4-component relativistic methods agreeing to within 1 pm on the bond distance of UO_2^{2+} [27]. The effects on the electronic spectra are more important but do not affect the comparison between different correlation methods that is the subject of the current paper. We will therefore focus exclusively on spin-free calculations to simplify the discussions, and refer to a previous paper by two of us for a more detailed discussion of the SO-CASP2 and SO-IHFSCC results for UO_2^{2+}. [27] We shall address spin-orbit effects on the spectra of NUN and NUO^+ in a subsequent publication.

2 Computational Details

All calculations were performed with spin-free relativistic methods using ADF2008 (and ADF2009 [46–48] for the (meta-)hybrid functionals), as well as with a development version of the DIRAC08 [49] program. To facilitate comparisons with the TDDFT calculations of van Besien and Pierloot [18] we used for UO_2^{2+} ion the same geometry (a U–O bond distance of 1.708 Å). The geometries of NUN and NUO^+ were optimized with the PBE exchange-correlation functional, the ADF TZ2P basis set and the all-electron scalar relativistic ZORA (Zero Order Regular Approximation) [50] Hamiltonian. The U–N distance in NUN molecule was determined to be 1.739 Å, whereas for NUO^+ it was found to be 1.698 Å. The U–O distance in NUO^+ is calculated to be 1.761 Å.

2.1 TDDFT

In the TDDFT calculations we applied the adiabatic approximation, where the frequency-dependent exchange-correlation kernel has been replaced by the local (in time) functional

derivatives of the frequency-independent functional. In ADF the ALDA approximation is used for all XC functionals, whereas for DIRAC[20] we used the full derivatives of the functionals (obtained via the XCFun DFT library[51]) in the XC kernel in addition to the ALDA approach. We note that, in the case of hybrid functionals, in both ADF and DIRAC the fractional Hartree-Fock exchange is always included in the TDDFT kernel.

For both ADF and DIRAC, we have evaluated the following functionals: LDA[52], PBE[53], BLYP[54–56], B3LYP[57], PBE0[58] as well as the SAOP model potential[59,60]. Additionally, the functionals M06, M06-L, M06-2X[61,62] were evaluated in the ALDA approximation using ADF, whereas CAM-B3LYP[63] was evaluated in DIRAC for both the ALDA and full (non-ALDA) TDDFT kernels.

In all calculations with ADF TZ2P basis sets (U:15s13p9d5f; O:5s3p1d1f)[64] were used, whereas for DIRAC we used the triple zeta basis set of Dyall[65] for the uranium atom (33s29p20d13f5g2h), and the uncontracted aug-cc-pVTZ basis set for oxygen and nitrogen (11s6p3d2f)[66,67]. We have used the scalar ZORA[50] Hamiltonian in ADF, and the spin-free Dirac-Coulomb[68] (DC) Hamiltonian in DIRAC. In the DC case the $(SS|SS)$ integrals have been approximated by a point charge model.[69]

Our work focused on five low-lying vertical excitations determined by DFT calculations. For UO_2^{2+} we studied transitions mainly consisting of excitations $3\sigma_u \rightarrow 1\phi_u$, $3\sigma_u \rightarrow 1\delta_u$, $2\pi_u \rightarrow 1\phi_u$, $3\sigma_g \rightarrow 1\phi_u$ and $3\sigma_g \rightarrow 1\delta_u$. For NUO^+ molecule the following dominant excitations were studied: $6\sigma \rightarrow 1\phi$, $6\sigma \rightarrow 1\delta$, $3\pi \rightarrow 1\phi$, $3\pi \rightarrow 1\delta$ and $5\sigma \rightarrow 1\phi$, while for NUN the dominant excitations are $3\sigma_u \rightarrow 1\phi_u$, $3\sigma_u \rightarrow 1\delta_u$, $3\sigma_g \rightarrow 1\phi_u$, $2\pi_u \rightarrow 1\phi_u$ and $3\sigma_u \rightarrow 4\sigma_g$.

2.2 CASPT2

CASPT2 calculations were carried out with the MOLCAS 7.4[70] program. For all CASPT2(MS-CASPT2)[34,35,71] calculations we utilized the scalar second-order Douglas-Kroll-Hess (DKH2) Hamiltonian[72,73], together with the (contracted) ANO-RCC basis sets, optimized specifically for this Hamiltonian: (26s23p17d13f5g3h) $\rightarrow$ [10s9p7d5f3g2h] for uranium, (14s9p4d3f2g) $\rightarrow$ [5s4p3d2f] for oxygen and (14s9p4d3f2g) $\rightarrow$ [4s3p2d1f] for nitrogen[74].

The most important point in the CASSCF calculation is the proper choice of active space. In the molecules investigated, the U-O and U-N bonds are formed out of the 6p, 7s, 5f, 6d orbitals of the uranium atom and the 2s and 2p orbitals of the oxygen and nitrogen atoms. While it would be ideal to take into account all molecular orbitals that are formed out of these atomic uranium, oxygen and nitrogen orbitals and correlate them in the CASPT2(MS-CASPT2) level, such an active space becomes too large to handle and we are forced to truncate the active space. It was possible to enlarge the active space for the UO_2^{2+} compound in comparison to the previous work by Réal[27], and we took into active space 12 electrons and 16 orbitals - CAS(12,16): $3\sigma_g$, $1\pi_g$, $2\pi_u$, $3\sigma_u$, $1\delta_u$, $1\phi_u$, $3\pi_u$, $4\sigma_g$, $4\sigma_u$ and $2\pi_g$. For NUO^+ and NUN molecules we also correlated 12 electrons and 16 orbitals - CAS(12,16), that is 5σ, 2π, 3π, 6σ, 1δ, 1ϕ, 7σ, 2δ, 4π and 8σ in case of NUO^+ and $3\sigma_g$, $1\pi_g$, $2\pi_u$, $3\sigma_u$, $1\delta_u$, $1\phi_u$, $4\sigma_g$, $3\pi_u$, $1\delta_g$ and $4\sigma_u$ in case of NUN. Due to technical problems encountered with MOLCAS 7.4 it was not possible to obtain the CAS(12,16) results for some of the higher-lying states of NUO^+, in order to obtain these energies we also employed a CAS(12,15) space in which the 7σ orbital was not taken in the active space.

In order to eliminate weakly intruding states in the second-order perturbation theory, we used the imaginary shift method[75] with a shift parameter of 0.25 Hartree when exploratory calculations indicated problems with intruder states.

2.3 IHFSCC

Intermediate Hamiltonian Fock space coupled cluster (IHFSCC)[36–38] calculations were performed with a development version of DIRAC08[49]. In those, the spin-free[68] DC Hamiltonian was used with the same uncontracted basis sets as described above for the TDDFT Dirac calculations.

In order to be consistent with our previous calculations on UO_2^{2+}, and due to the fact that in their ground state these molecules are well described by a single determinant, we have essentially followed the procedure outlined in[27](with the difference that we used 1.708 Å as the U-O bond length); that is, we have utilized the "one particle, one hole" sector $(1h,1p)$ of Fock space to obtain the excitation energies, and have included in the correlated calculations orbitals with energies (in a.u.) $\varepsilon \in [-3.00;20.00]$, which correspond to 12 occupied and 253 (252) virtual orbitals for NUN (NUO^+).

In Fock space calculations it is necessary to subdivide the space spanned by the active orbitals in two subspaces: the model or P space, containing the active valence orbitals which are directly involved in the electronic excitations and the complementary Q space that includes the remaining "correlation-active" orbitals. As we are employing a formulation based on an intermediate Hamiltonian[76], the P space is further divided into a main model (P_m) space and an intermediate model (P_i) space that is not dressed and serves as a buffer between the P_m and Q spaces, in order to alleviate problems with the so-called intruder states (further details can be found in[27] and references therein). One must keep in mind, however, that accurate solutions are only obtained for states dominated by P_m components.

Thus, in the definition of the Fock space used here, P contains all the occupied plus the 63 lowest-lying virtuals (for NUN, 29 virtuals are contained in gerade irreducible repre-

sentations, and 34 in ungerade ones), whereas the remaining virtuals have been assigned to the Q space. As for the partition into P_m and P_i orbital spaces we have, for the occupied orbitals, the five innermost orbitals in P_i – which correspond to $\{1\sigma_g, 1\sigma_u, 1\pi_u, 2\sigma_g\}$ for NUN and $\{1\sigma, 2\sigma, 1\pi, 3\sigma\}$ for NUO^+ – and the remaining seven orbitals in P_m – namely $\{3\sigma_g, 2\sigma_u, 3\sigma_u, 1\pi_g, 2\pi_u\}$ for NUN and $\{4\sigma, 5\sigma, 6\sigma, 2\pi, 3\pi\}$ for NUO^+.

For the virtuals the P_m active spaces correspond to 31 (22) orbitals for NUN (NUO^+), assuring that the resulting lowest-lying excited states are dominated by P_m components. These orbitals correspond roughly to about two to three lowest-lying $\phi(=\phi_u)$ and $\delta(=\delta_u, \delta_g)$ orbitals of Uranium, apart from the same number of π and twice as many σ orbitals. The difference between these sets is due to the difference in charge for both systems and the nature of the Hartree-Fock virtuals; contrary of what is obtained with DFT, the ϕ, δ orbitals of Uranium are not the lowest-lying ones – a number of π, σ orbitals lie below and in between the former and had to be included in the model space as well.

3 Wavefunction Benchmark Calculations

As the main goal of this work is assessing the performance of TDDFT by comparison to benchmark WFT values we will begin with a brief discussion of the two WFT methods employed here, before having a closer look at the actual DFT and TDDFT results.

3.1 Electronic structure from IHFSCC

We refer the reader to the paper of Réal and coworkers[27] for a detailed discussion of the UO_2^{2+} IHFSCC calculations. These calculations were done at a different bond length, leading to slightly different numbers in Table 1, compared to those previously reported (see Table 2 of the aforementioned paper), but analysis of the wavefunctions at both geometries yields essentially the same picture. For UO_2^{2+} the lowest Φ_g and Δ_g states are dominated by excitations of the $\sigma_u \rightarrow \phi_u$ and $\sigma_u \rightarrow \delta_u$ kind, respectively, while the Γ_g states arises from predominantly $\pi_u \rightarrow \phi_u$ excitation. The Φ_u and Δ_u states correspond to exciations from $\sigma_g \rightarrow \phi_u$ and $\sigma_g \rightarrow \delta_u$, respectively.

For NUN, the Φ_g and Φ_u states in Table 3, differ essentially in the occupied σ orbital (σ_u for the first and σ_g for the second). These two σ orbitals, in turn, differ only in the degree of contributions from the orbitals centered on N and U, with σ_u having more U character and the σ_g having more N character. And, since the ϕ_u orbital is essentially a pure f from U, we can argue that the two transitions have different degrees of charge-transfer character. The other higher-lying excitations are dominated by $\pi_u \rightarrow \phi_u$ (for Γ_g, where π_u has dominant contributions from N, but still some U character), and $\sigma_u \rightarrow \sigma_g$ (for Σ_u, where both σs have N and U character).

For NUO^+, shown in Table 2, the picture is similar, but having as significant differences that the lowest Φ and Δ states are made up of excitations to the uranium ϕ, δ from σ orbitals with either N-U character or U-O character, whereas the Γ and Φ arise from excitations to the same uranium ϕ, δ from a π orbital with N-U character.

The Hartree-Fock virtual orbitals correspond to a system with one electron added relative to the reference determinant. While this is optimal for calculating electron affinities, it is not so for excitation energies calculated within the $(1h, 1p)$ sector of Fock space. In order to compare to the TDDFT results, the model spaces (P and P_m) should include the δ_u, ϕ_u orbitals. These are the lowest virtuals for UO_2^{2+}, both for Hartree-Fock and DFT, but the decreasing charge on the metal in NUO^+ and particularly in NUN places other orbitals at lower energy. For instance, for NUO^+, three σ and two π virtual orbitals have lower energies than the relevant δ, ϕ orbitals, while for NUN several (e.g. two σ_u, three π_u, three σ_g and one π_g) orbitals are in between the HOMO and the δ_u, ϕ_u. These differences illustrate the need for increased model spaces in this work, compared to UO_2^{2+}, for which the δ_u and ϕ_u are the lowest-lying virtuals.

A related difference to the UO_2^{2+} case is the extent to which the participation of a second set of δ, ϕ virtuals is important for NUO^+ and NUN. This is due to the energy separation of the first and second δ and ϕ virtuals, which for UO_2^{2+} is of about 8 eV, but decreases to within 1.5 – 2 eV for NUO^+ and NUN, making these virtuals more important for orbital relaxation in the latter case.

Lastly, we note that in all three cases the T_1 diagnostic[77] for the $(0h, 0p)$ sector (which here is equivalent to a conventional CCSD calculation), namely 0.045 for UO_2^{2+}, 0.048 for NUO^+ and 0.049 for NUN, is rather similar and a bit higher than what is usually considered an indicator (< 0.02) of single-reference character in light systems. This is typical for heavy elements, and should not be taken as an indication of multi-reference character.

3.2 CASPT2 electronic structure

The CASSCF wavefunction analysis points to ground-states of essentially single reference character, with weights for the HF determinant of about 0.86, 0.92 and 0.91 for UO_2^{2+}, NUO^+ and NUN respectively. Also of importance is the fact that the determinants which contribute to the remaining 0.10 are made up of double excitations, and therefore do not point to important orbital relaxation effects[78].

CASPT2 provides in a fairly straightforward manner information about the bond orders in the ground state (2.935(U–O) for UO_2^{2+}, 2.952(U–N) for NUN, and 1.957(U–O) and 2.977

(U–N) for NUO^+). Changes in the electron density upon excitation can be studied by means of an analysis of the Mulliken charges for each excited state. From these charges, summarized in Table 4, we can see that there is a general trend of displacing a small amount of density towards the uranium atom in comparison to the ground state. This effect is more systematic (in the sense of all states showing a transfer of charge from the ligands to the uranium) in the case of UO_2^{2+} than for NUN, for which only the Σ_u states have a rather pronounced ligand to uranium charge transfer relative to the ground state. For NUO^+ the most important effect is the migration of charge from one end of the molecule (the O atom) to the other (the N atom) rather than a net movement of charge towards the central atom.

3.3 Comparison of WFT excitation energies

In a previous investigation of the performance of IHFSCC and CASPT2 in calculating the electronic spectrum of UO_2^{2+} [27], two of us observed that CASPT2 typically shows discrepancies with respect to IHFSCC for individual excitation energies within a range of 0.1–0.4 eV. Furthermore, for the lowest Φ_g and Δ_g, both singlet and triplet, CASPT2 overestimated the excitation energies, whereas for higher-lying states the opposite is true. The singlet-triplet splittings, however, were quite similar for both methods. The same general trends are seen here for NUO^+ and NUN in Tables 2 and 3, respectively. The differences between individual excitation energies for both methods are typically in the 0.1–0.3 eV range. We may conclude that the two WFT methods give the same semi-quantitative result and will take IHFSCC as the reference method, given its more systematic treatment of the excited states and inclusion of dynamic correlation effects beyond second order perturbation theory.

4 The performance of DFT and TDDFT

Our TDDFT tests were focused on a subset of XC functionals, covering the following basic classes: LDA, GGAs (PBE, BLYP) and meta-GGAs (M06-L), hybrids (B3LYP and PBE0, with 20 and 25% of HF exchange, respectively) and meta-hybrids (M06 and M06-2X, with 27 and 54% of HF exchange, respectively), model potentials (SAOP) and range-separated hybrids (CAM-B3LYP).

We have chosen to represent all systems by restricted (closed-shell) Kohn-Sham calculations, given the evidence both from our wavefunction calculations and from previous studies (e.g. that of Kaltsoyannis [10], Pierloot and coworkers [18,25], those of Réal and coworkers [26] and that of Fromager [78] and coworkers, that this yields a proper description for their ground states. The suitability of this approach for uranyl was further demonstrated in the recent Kramers-restricted TDDFT calculations by Bast *et al.* [20].

4.1 Ground-state electronic structure

Before discussing the performance of (TD)DFT for the different electronically excited states, it is instructive to discuss the molecular orbitals (MOs) and the chemical bonding. The essentials of bonding in the actinyls are nicely summarized in a review by Denning [79]; in particular, for UO_2^{2+} the currently accepted picture, in terms of the highest-lying occupied MOs, is that of a system of σ,π orbitals arising from the combination of oxygen $2p$ orbitals and the $5f,6p$ orbitals of uranium, ordered as $\pi_g > \pi_u > \sigma_g > \sigma_u$. In UO_2^{2+} the contribution from the uranium $6p$ shows up in the relatively large gap between the σ orbitals, due to the repulsion between σ_u and $6p$, [80] a so-called "pushing from below" interaction.

To our knowledge only the aforementioned work of Kaltsoyannis has paid attention to the valence MO picture of NUN and NUO^+. Using a GGA functional (PB86), he found: (a) the same orbital ordering for NUN and UO_2^{2+}, but with a smaller (larger) energy gap between the σ (π) orbitals; and (b) an ordering of type $\pi > \sigma > \pi > \sigma$ for NUO^+, with the (energetically) lower π,σ pair mostly centered over the U–O bond, whereas the HOMO and HOMO-1 are mostly centered over the U–N bond. This picture is qualitatively consistent already with the Hartree-Fock results, but in order to obtain reliable information about the orbital ordering electron correlation should also be included. To remain within an orbital picture, we shall do so by comparing the vertical ionization potentials (IPs) obtained from the $(1h,0p)$ sector in the IHFSCC calculations to those obtained from DFT.

The DFT IPs are here taken as approximations to the negative of the respective orbital energies, and while this is strictly valid only for the HOMO, [81] our results (shown in Table 5) indicate that this is a good approximation, in line with the findings of Chong and coworkers [82].

4.1.1 Describing the occupied space From the numbers in Table 5, we can confirm that the orbital scheme outlined above is maintained for all three molecules, with one exception for M06-2X (which for NUN places the σ_u orbital below the σ_g). On the other hand, we observe significant quantitative differences as far as the differences in energy between orbitals (for a given molecule) are concerned. These are very much dependent on the type of functional in use (LDA/GGA, hybrids, metaGGAs/hybrids, etc); for instance, the energy difference between the HOMO and HOMO-1 for NUN or UO_2^{2+} can be halved just by going from GGAs to hybrids. Also striking is the fact that there is very little difference (of the order of 0.1 eV) in energy between σ_g and σ_u for IHFSCC in the case of UO_2^{2+}, whereas the DFT calculations yield differences between 0.3 and 1 eV.

These numbers are rather insensitive to the Hamiltonian; in general, we observe discrepancies no larger than 0.1 eV (but generally lower than 0.05 eV) between the ZORA and DC Hamiltonians (keeping in mind that one also might have effects due to the different basis sets used by ADF and DIRAC). This is in line with experience that approximate (but computationally efficient) two-component relativistic schemes such as ZORA yield accurate valence energies.

Looking at the performance of the various DFT approaches, we find the best agreement with IHFSCC for the SAOP potential. Comparing the DC values it shows errors in the range -0.3 – 0.5 eV. It is followed by CAM-B3LYP and M06-2X, which systematically underestimate the IPs by about 1 eV and 1–1.5 eV, respectively. Next come two blocks, one grouping the remaining (meta)hybrids, and another encompassing LDA and the (meta)GGAs, which underestimate the IPs by about 3 and 4 eV, respectively.

While other factors, like the correlation part of the functionals, also play a role these trends may be rationalized by considering the degree to which self-interaction errors (SIE) are eliminated from each functional. The reader is referred to refs.[83–86] for discussion of the self-interaction problem. Important to note in the present context is the inability of approximate functionals to, in a one-electron picture (1-SIE), correctly cancel out the Coulomb interaction of the electron with itself through the exchange interaction (which in Hartree-Fock theory is exactly cancelled out) or, in a many-electron case (N-SIE), to properly describe the discontinuity of the derivative of the total energy with respect to (fractional) changes in particle number (the so-called integer discontinuity). The inability of GGAs to properly represent such discontinuities in the energy and exchange-correlation (xc) potential (the latter denoted here by Δ_{xc}) have been shown to be behind the failures of TDDFT in describing charge-transfer excitations[87], or to reproduce the correct asymptotic behavior of the exchange-correlation potential[88,89]. The latter defect is remedied by model potentials with the correct asymptotic (long-range) behavior, like LB94[60] and SAOP[59].

Based on the analysis of Teale and coworkers[90], valid for the case of pure functionals, we can estimate the value of Δ_{xc} from the relation

$$\Delta_{xc} = 2(I^0 + \varepsilon_{\mathrm{HOMO}}) \quad (1)$$

where I^0 is a reference ionization potential (taken to be the IHFSCC value here) and $\varepsilon_{\mathrm{HOMO}}$ is the Kohn-Sham orbital energy for the HOMO of the molecules (with the factor two arising from the assumption that, instead of a discontinuity, (meta)GGAs will exhibit an averaged potential over such discontinuity). From the differences between the LDA or GGAs and IHFSCC in Table 5 one sees that Δ_{xc} may have values of up to 8 eV, an indication that the effect of the integer discontinuity on the spectra of these systems is potentially large. We furthermore note that the asymptotically correct SAOP potential indeed provides a good agreement with the IHFSCC values.

An alternative to imposing the proper asymptotic behavior with a model potential is to introduce non-locality and reduce SIE is via the inclusion of Hartree-Fock exchange (as in hybrid functionals), via an explicit dependence of the functional on the kinetic energy (metaGGAs) or a combination of both (metahybrids). This is also done in range-separated hybrids such as CAM-B3LYP or others[91,92], that offer a more detailed control over the incorporation of exact exchange than is possible in conventional hybrids[84,93,94]. While the analysis of Teale is not applicable to (meta)hybrids, their better performance (in particular when compared to the analogous GGA, as one can then suppose similar errors due to electron correlation or other factors), does indeed suggest improvements relative to the non-hybrid functionals.

4.1.2 Remarks on the virtual space A detailed discussion concerning the representation of the virtual orbital space will not be made here. The main reason for that lies at the very different meaning of the virtual orbital energies[95] when pure (e.g. LDA or (meta)GGAs) or hybrid functionals are employed. It is well-known that for pure functionals the virtual orbital energies are good approximations to the ionization potentials of excited states, whereas in Hartree-Fock they represent approximations to electron affinities. For hybrids they are thus somewhere in between these two values making it difficult to compare these values with the IHFSCC values (that strictly represent electron affinities).

A consequence of the difference between Hartree-Fock and pure DFT is that one finds, for the GGA functionals employed here, the low-lying virtuals to be uranium-centered f_ϕ and f_δ orbitals (to which we will observe the transitions from the occupied σ,π orbitals discussed above), whereas for the hybrids these are often found higher in energy than other orbitals such as the σ and π antibonding orbitals.

4.2 The performance of different functionals for the excited states

All investigated XC functionals were subsequently compared to the wave function methods in Tables 1 (UO_2^{2+}), 2 (NUO^+) and 3 (NUN), which are known to perform very well for molecules containing heavy elements[19,27,39,41,42]. Since previous works indicate that IHFSCC energies are generally in better agreement with experiment than those from CASPT2, we chose to employ the former as our reference.

The tables contain, apart from the individual excitation energies and singlet-triplet splittings, the mean unsigned (MUE) and largest absolute (Max) errors with respect to IHFSCC for each molecule. We also provide a global picture in Figure 1,

where the (signed) errors are depicted for each individual excitation.

4.2.1 General trends The statistical measures help to identify trends and we start discussing the MUE. For that, LDA and the GGAs considered show essentially the same results for all molecules, namely large underestimations with GGAs showing no clear improvement over LDA. The meta-GGA M06–L on the other hand does show improvement over both LDA and GGAs, almost halving the error. For the (meta)hybrids the errors are smaller still, about four times smaller than those of GGAs or LDA. We thereby note that whereas for NUN and UO_2^{2+} the excitation energies are generally underestimated, for NUO^+ some functionals also show slight overestimations.

The B3LYP functional shows somewhat larger MUEs than PBE0 or M06(XALDA). The latter two show nearly identical results which is not so surprising as M06 bears a number of similarities to PBE0 (about the same amount of Hartree–Fock exchange, and exchange and correlation functionals based on those of PBE). It is nevertheless unfortunate that the higher flexibility in the functional form available for M06 does not translate into better accuracy than observed for PBE0. This may be due to the ALDA approximation employed in the current ADF implementation of this functional, however.

The M06-2X(XALDA) functional, in spite of having the same functional form as M06 (except for the amount of Hartree-Fock exchange), shows a worse performance than B3LYP, again indicating the important role played by the exchange energy. The model potential (SAOP) performs comparably to M06-2X(XALDA), while the range-separated (CAM-B3LYP) functional tends to show yet an improvement over PBE0 or M06. Furthermore, CAM-B3LYP generally matches the performance of CASPT2, even slightly outperforming it for NUN and UO_2^{2+}.

Nearly the same ranking of functional performance is seen for the largest absolute errors (Max), which are generally two to three times larger than the corresponding MUEs. The superior performance of (meta)hybrids and CAM-B3LYP compared to LDA or GGAs is evident for all three molecules, and it is interesting to see that, while the (meta)hybrids show a sightly better agreement with IHFSCC for NUN and UO_2^{2+} in comparison to NUO^+, for (meta)GGAs the opposite is true.

We believe that, as stated above for the ionization potentials, the large errors seen for LDA and GGAs have to do with a poor description of exchange energies, that are quite different for the ground and excited states. The xc kernel plays a significant role in determining the accuracy here, and in it, the amount of HF exchange is important as the differences between M06(XALDA) and M06-2X(XALDA), and the similarities between PBE0(XALDA) and M06(XALDA) can attest. However, it remains to be seen whether or not the same will hold for other actinide compounds, especially in connection to typical charge-transfer or Rydberg-type excitations (and where one would expect CAM-B3LYP to clearly outperform the other hybrids).

Providing an understanding of the differences in standard deviation between the different groups of functionals, on the other hand, seems to be a much more difficult task. We can at this time only speculate that, at least to some extent, N-SIE effects that affect the various exited states differently will be important. In that case, one could expect that calculations with functionals that show large N-SIE, as is the case with GGAs [84,93,94] would then exhibit larger standard deviations. In this respect, the SAOP potential is perhaps an interesting example. We have already discussed that SAOP reduces the SIE by correcting the long-range part of the potential. However, since SAOP was conceptualized to be used with the ALDA approximation, the errors inherent to the LDA functional find themselves back into the response calculation (as indicated by the large standard deviations for the excitation energies). These errors are incidentally of about the same order of any other calculations with (meta)GGAs and, more generally, of calculations with the ALDA kernel.

Also worth noting here is that, in spite of its better performance on the mean error compared to the investigated (local) GGA functionals, M06–L(ALDA) ultimately remains more in line with them than with the (meta)hybrids. At this point we cannot exclude that improvements could be seen if we departed from the ALDA kernel given which, as discussed below, can have significant effects on individual excitations.

4.2.2 ALDA or Exact derivatives in the kernel? In order to judge whether the ALDA approximation changes significantly the electronic spectrum of investigated molecules we consider calculations with the PBE, PBE0, BLYP, B3LYP and CAM-B3LYP xc functionals with and without ALDA. The effect of the ALDA approximation is depicted in Figure 2 for the lowest two excitations of each of the molecules considered.

From Figure 2 and the values in Tables 1 through 3 we conclude that for the singlet states the effect of ALDA is small, but a surprisingly large discrepancy occurs for the triplet states, especially in the lowest electronic transitions (differences up to 0.4 eV). For the higher transitions the effect is smaller (difference up to 0.04) in all investigated molecules and functionals. PBE0 and B3LYP suffer somewhat less than PBE and BLYP from the ALDA approximation for the triplet energies, due to the fractional Hartree–Fock exchange still present in the kernel. We may thus expect that the ALDA approximation also has a large effect on triplet energies for the M06-L functional (for which an implementation of the full kernel is not yet available) but less so for M06 and in particular M06-2X which contain a large portion of Hartree–Fock exchange. Finally we note that by its construction as a model potential, it

is difficult to remove the ALDA ansatz for SAOP, and here the large errors (see Fig. 1) in the triplet energies can not be easily remedied.

4.2.3 Comparison to previous calculations and benchmarks The results discussed above are in line with those from recent benchmark calculations on different molecular databases that do not include molecules containing heavy centers[96–102]. In particular, the recent comparison of the M06 family to other functionals by Jacquemin and coworkers[99] points to the same general trends seen here: M06 does show the best overall performance in the family and is close to PBE0, while M06-2X shows a slightly worse performance. They also show that M06–L outperform different GGAs, but still cannot match the accuracy of conventional hybrids functionals such as B3LYP.

It is difficult to directly compare our MUE values and those of Jacquemin and coworkers[99], or those of Silva–Junior and coworkers[101,102], due to the different methodologies used to obtain the reference values (and the extent to which basis set effects can influence the WFT[102] or TDDFT[103] results). We can nevertheless observe, for hybrids such as M06 or B3LYP, a rather good agreement between our MUE and those of the literature (and similarly for the unsigned errors shown in Fig. 1). For GGAs, on the other hand, the values in the literature seem to be much smaller than ours. We are not able at this time to say whether this is definitely a degradation of performance for the GGAs for actinides or whether this is an artifact due to the limited size of our benchmark set.

Considering now calculations on molecules with heavy elements we confirm, for the uranyl spectrum, the observations of Bast *et al.*[20] who included spin-orbit coupling and compared the performance of functionals relative to the LR-CCSD results of Réal and coworkers[26]. While the latter have not considered the M06 family of functionals, they also reported a lowest MUE for CAM-B3LYP with LDA and GGAs severely underestimating the excitation energies.

Comparing our results to the benchmark calculations of Zhao and Truhlar (Table 17 in[62]) where a broad range of excitation energies calculated with different functionals are compared to reference values, we do not see the same drastic improvement going from hybrid functionals (B3LYP, PBE0) to metahybrids (M06, M06-2X). In our application, M06-2X brings the excitation energies too close to the Hartree–Fock values and introduces significant errors. Most likely this discrepancy between our particular molecules and excitations and the data presented by Zhao and Truhlar is due to the fact that we do not include Rydberg or extreme charge transfer states in our benchmark. In these cases it is crucial to use functionals with a correct treatment of the nonlocality of the change in the electron density. Based on our results we cannot recommend M06-2X for the systems and excitations studied in this work, despite its good performance in other benchmarks.

5 Conclusions

We investigated the performance of different classes of approximate exchange-correlation functionals in describing ten low-lying valence excitations for the uranyl ion (UO_2^{2+}) and two isoelectronic analogs, NUO^+ and NUN by comparing them to wavefunction calculations (CASPT2 and Fock-space coupled cluster). A marked characteristic of such systems, all of which are closed-shell species in the ground state, is that the low-lying excited states under consideration correspond to excitation from the σ,π bonding orbitals to unoccupied orbitals which are essentially Uranium f orbitals.

We can identify the following trends regarding the functional's performance: a) LDA and (meta)GGAs show somewhat larger mean errors than (meta)hybrids or model potential such as SAOP; however, the standard deviation for those is significantly larger than for the (meta)hybrids. b) one hardly observes an improvement for metaGGAs or meta hybrids in comparison to GGAs or hybrids, with perhaps the exception of the improvement of the mean error for M06-L over the GGAs considered; and c) The performance of M06, PBE0 and CAM-B3LYP approaches that of CASPT2, both in terms of relatively small MAEs and standard deviations for the excitations. Of course, with only three molecules studied, one cannot rule out that the present agreement is fortuitous, but based on this benchmark M06, PBE0 and especially CAM-B3LYP appear appropriate for quantitative studies of actinide spectroscopy. Other hybrid functionals such as M06-2X and B3LYP are suited for (semi)quantitative or qualitative work, but we would strongly argue against employing non-hybrid (meta)GGAs even for qualitative investigations of excited states of actinyls.

In view of those trends, we believe that, while the correlation functional does play an important role in the accuracy of results – as seen in the differences between different functionals of same kind (GGAs, hybrids etc), what appears to be a critical factor governing the accuracy of the functionals tested is the degree of non-locality introduced through inclusion of HF exchange in hybrids or meta-hybrids. We could thereby rationalize why: i) hybrids outperform their pure GGA counterparts; ii) M06-L(ALDA) shows some improvement over the GGAs regarding the mean error but not in the standard deviation; iii) the SAOP model yields excellent ionization potentials and mean errors for the excitation energies but has standard deviations similar to GGAs.

It is also clear that one must go beyond the ALDA approximation, given the rather large differences observed between the low-lying triplet states. Equally (or perhaps more) important, however, is that non-local effects should also be incorporated to the exchange-correlation kernel, as done for all

(meta)hybrids and CAM-B3LYP, if one wishes to approach the accuracy of methods such as CASPT2.

It is, finally, interesting to note that for excitation energies the choice of relativistic (spin-free) Hamiltonian is almost irrelevant, so one can safely investigate the spectra of actinide-containing molecules with the more approximate two-component methods (such as ZORA), instead of using four-component approaches.

6 Acknowledgments

The authors thank Dr. Florent Réal, Dr. Radovan Bast, and Dr. Erik van Lenthe for helpful discussions on the practical aspects of carrying out the MOLCAS CASPT2 and the DIRAC and ADF TDDFT calculations, respectively. The authors acknowledge financial support from The Netherlands Organization for Scientific Research (NWO) via the Vici program, as well as computer time provided by the Dutch National Computing Facilities (NCF) at the Huygens and LISA facilities at SARA.

ASPG also acknowledges the use of computational resources from CINES ("Centre Informatique National de l'Enseignement Supérieur") and CCRT ("Centre de Calcul Recherche et Technologie"), under grant "phl2531".

References

1 K. Nash, *Solvent Extr. Ion Exch.*, 1993, **11**, 11729.
2 K. L. Nash, R. E. Barrans, R. Chiarizia, M. L. Dietz, M. Jensen and P. Rickert, *Solvent Extr. Ion Exch.*, 2000, **18**, 605.
3 E. P. Horwitz, D. G. Kalina, H. Diamond, G. F. Vandegrift and W. W. Schulz, *Solvent Extr. Ion Exch.*, 1985, **3**, 75.
4 G. Schreckenbach and G. A. Shamov, *Acc. Chem. Res.*, 2010, **43**, 19.
5 M. Pepper and B. E. Bursten, *Chem. Rev.*, 1991, **91**, 719–741.
6 Q.-J. Pan, G. A. Shamov and G. Schreckenbach, *Chem. Eur. J.*, 2010, **16**, 2282.
7 M. del C. Michelini, J. Marçalo, N. Russo and J. H. Gibson, *Inorg. Chem.*, 2010, **49**, 3836.
8 N. Iché-Tarrat and C. J. Marsden, *J. Phys. Chem. A*, 2008, **112**, 7632.
9 G. S. Groenewold, A. K. Gianotto, M. E. McIlwain, M. J. van Stipdonk, M. Kullman, D. T. Moore, N. Polfer, J. Oomens, I. Infante, L. Visscher, B. Siboulet and W. A. de Jong, *J. Phys. Chem. A*, 2008, **112**, 508.
10 N. Kaltsoyannis, *Inorg. Chem.*, 2000, **39**, 6009.
11 N. Ismail, J.-L. Heully, T. Saue, J.-P. Daudey and C. J. Marsden, *Chem. Phys. Lett.*, 1999, **300**, 296.
12 T. Privalov, P. Macak, B. Schimmelpfennig, E. Fromager, I. Grenthe and U. Wahlgren, *J. Am. Chem. Soc.*, 2004, **126**, 9801.
13 G. A. Shamov, G. Schreckenbach and T. N. Vo, *Chem. Eur. J.*, 2007, **13**, 4932.
14 G. Schreckenbach and G. A. Shamov, *Acc. Chem. Res.*, 2010, **43**, 19.
15 A. Rosa, E. J. Baerends, S. J. A. van Gisbergen, E. van Lenthe, J. A. Groeneveld and J. G. S. Snijders, *J. Am. Chem. Soc.*, 1999, **121**, 10356.
16 S. J. A. van Gisbergen, J. A. Groeneveld, A. Rosa, J. G. Snijders and E. J. Baerends, *J. Phys. Chem. A*, 1999, **103**, 6835.
17 S. J. A. van Gisbergen, A. Rosa, G. Ricciardi and E. J. Baerends, *J. Chem. Phys.*, 1999, **111**, 2499.
18 K. Pierloot, E. van Besien, E. van Lenthe and E. J. Baerends, *J. Chem. Phys.*, 2007, **126**, 194311.
19 F.-P. Notter, S. Dubillard and H. Bolvin, *J. Chem. Phys.*, 2008, **128**, 164315.
20 R. Bast, H. J. A. Jensen and T. Saue, *Inter. J. Q. Chem.*, 2009, **109**, 2091.
21 S. Fortier, G. Wu and T. W. Hayton, *J. Am. Chem. Soc.*, 2010, **132**, 6888.
22 D. R. Brown and R. G. Denning, *Inorg. Chem.*, 1996, **35**, 6158.
23 L. P. Spencer, P. Yang, B. L. Scott, E. R. Batista and J. M. Boncella, *Inorg. Chem.*, 2009, **48**, 2693.
24 S. Fortier and T. W. Hayton, *Coord. Chem. Rev.*, 2010, **254**, 197.
25 K. Pierloot and E. van Besien, *J. Chem. Phys.*, 2005, **123**, 204309.
26 F. Réal, V. Vallet, C. Marian and U. Wahlgren, *J. Chem. Phys.*, 2007, **127**, 214302.
27 F. Réal, A. S. P. Gomes, L. Visscher, V. Vallet and E. Eliav, *J. Phys. Chem. A*, 2009, **113**, 12504.
28 F. Ruipérez, C. Danilo, F. Réal, J.-P. Flament, V. Vallet and U. Wahlgren, *J. Phys. Chem. A*, 2009, **113**, 1420.
29 R. Bast, *Ph.D. thesis*, l'Université Luis Pasteur, Strasburg, 2007.
30 S. Matsika, Z. Zhang, S. R. Brozell, J.-P. Blaudeau, Q. Wang and R. M. Pitzer, *J. Phys. Chem. A*, 2001, **105**, 3825.
31 M. Zhou, N. Ismail, C. Marsden and L. Andrews, *J. Phys. Chem. A*, 2000, **104**, 5495.
32 L. Gagliardi and B. O. Roos, *Chem. Soc. Rev.*, 2007, **36**, 893.
33 R. D. Hunt, J. T.Yustein and L. Andrews, *J. Chem. Phys.*, 1993, **98**, 6070.
34 K. Andersson, P.-A. Malmqvist, B. O. Roos, A. J. Sadlej and K. Wolinski, *J. Phys. Chem.*, 1990, **94**, 5483.
35 K. Andersson, P.-A. Malmqvist and B. O. Roos, *J. Chem. Phys.*, 1992, **96**, 1218.
36 A. Landau, E. Eliav, Y. Ishikawa and U. Kaldor, *J. Chem. Phys.*, 2000, **113**, 9905.
37 A. Landau, E. Eliav, Y. Ishikawa and U. Kaldor, *J. Chem. Phys.*, 2001, **115**, 6862.
38 L. Visscher, E. Eliav and U. Kaldor, *J. Chem. Phys.*, 2001, **115**, 9720.
39 I. Infante, A. S. P. Gomes and L. Visscher, *J. Chem. Phys.*, 2006, **125**, 074301.
40 I. Infante, E. Eliav, M. J. Vilkas, Y. Ishikawa, U. Kaldor and L. Visscher, *J. Chem. Phys.*, 2007, **127**, 124308.
41 G. L. Macchia, I. Infante, J. Raab, J. K. Gibson and L. Gagliardi, *Phys. Chem. Chem. Phys.*, 2008, **48**, 7278.
42 A. S. P. Gomes, L. Visscher, H. Bolvin, T. Saue, S. Knecht, T. Fleig and E. Eliav, *J. Chem. Phys.*, 2010, **133**, 064305.
43 R. J. Bartlett and M. Musiał, *Rev. Mod. Phys.*, 2007, **79**, 291–351.
44 L. Meissner and M. Musiał, *Recent Progress in Coupled Cluster Methods*, Springer Sience+Business Media B.V., 2010, p. 395.
45 V. V. Ivanov, D. I. Lyakh and L. Adamowicz, *Phys. Chem. Chem. Phys.*, 2009, **11**, 2355–2370.
46 G. te Velde, F. M. Bickelhaupt, S. J. A. van Gisbergen, C. F. Guerra, E. J. Baerends, J. G. Snijders and T. Ziegler, *J. Comput. Chem.*, 2001, **22**, 931.
47 C. F. Guerra, J. G. Snijders, G. te Velde and E. J. Baerends, *Theor. Chem. Acc*, 1998, **99**, 391.
48 ADF2009.01, SCM, Theoretical Chemistry, Vrije Universiteit, Amsterdam, The Netherlands, http://www.scm.com.
49 DIRAC, a relativistic ab initio electronic structure program, Release DIRAC08 (2008), written by L. Visscher, H. J. Aa. Jensen, and T. Saue, with new contributions from R. Bast, S. Dubillard, K. G. Dyall, U. Ekström, E. Eliav, T. Fleig, A. S. P. Gomes, T. U. Helgaker, J. Henriksson, M. Iliaš, Ch. R. Jacob, S. Knecht, P. Norman, J. Olsen, M. Pernpointner, K. Ruud, P. Sałek, and J. Sikkema (see http://dirac.chem.sdu.dk).
50 E. van Lenthe, E. J. Baerends and J. G. Snijders, *J. Phys. Chem.*, 1993, **99**, 4597.
51 U. Ekström, L. Visscher, R. Bast, A. J. Thorvaldsen and K. Ruud,

J. Chem. Theory Comput., 2010, **6**, 1971.
52 S. H. Vosko, L. Wilk and M. Nusair, *Can. J. Phys.*, 1980, **58**, 1200.
53 J. P. Perdew, K. Burke and M. Ernzerhof, *Phys. Rev. Lett.*, 1996, **77**, 3865.
54 A. Becke, *Phys. Rev. A*, 1988, **38**, 3098.
55 C. Lee, W. Yang and R. G. Parr, *Phys. Rev. B*, 1988, **37**, 785.
56 B. G. Johnson, P. M. W. Gill and J. A. Pople, *J. Chem. Phys.*, 1993, **98**, 5612.
57 P. J. Stephens, F. J. Devlin, C. F. Chabalowski and M. J. Frisch, *J. Phys. Chem.*, 1994, **98**, 11623.
58 M. Ernzerhof and G. Scuseria, *J. Chem. Phys.*, 1999, **110**, 5029.
59 P. R. T. Schipper, O. V. Gritsenko, S. J. A. van Gisbergen and E. J. Baerends, *J. Chem. Phys.*, 2000, **112**, 1344.
60 R. van Leeuwen and E. J. Baerends, *Phys. Rev. A*, 1994, **49**, 2421.
61 Y. Zhao and D. G. Truhlar, *J. Chem. Phys.*, 2006, **125**, 13126.
62 Y. Zhao and D. G. Truhlar, *Theor. Chem. Acc*, 2008, **120**, 215.
63 T. Yanai, D. P. Tew and N. C. Handy, *Chem. Phys. Lett.*, 2004, **393**, 51.
64 E. van Lenthe and E. J. Baerends, *J. Am. Chem. Soc.*, 2003, **24**, 1142.
65 K. G. Dyall, *Theor. Chem. Acc*, 2007, **117**, 483.
66 T. H. Dunning, *J. Chem. Phys.*, 1989, **90**, 1007.
67 R. A. Kendall, T. H. Dunning and R. Harrison, *J. Chem. Phys.*, 1989, **96**, 6796.
68 L. Visscher and T. Saue, *J. Chem. Phys.*, 2000, **113**, 3996.
69 L. Visscher, *Theor. Chem. Acc*, 1997, **98**, 68.
70 G. Karlström, R. Lindh, P.-A. Malmqvist, B. O. Roos, U. Ryde, V. Veryazov, P.-O. Widmark, M. Cossi, B. Schimmelpfennig, P. Neogrady and L. Seijo, *Comput. Mat. Sci.*, 2003, **28**, 222.
71 J. Finleya, P.-A. Malmqvist, B. O. Roos, and L. Serrano-Andrés, *Chem. Phys. Lett.*, 1998, **288**, 299.
72 N. Douglas and N. M. Kroll, *Ann. Phys.*, 1974, **82**, 89.
73 B. A. Hess, *Phys. Rev. A*, 1986, **33**, 3742.
74 P.-O. Widmark, P.-A. Malmqvist and B. O. Roos, *Theor. Chem. Acc*, 1990, **77**, 291.
75 N. Forsberg and P.-A. Malmqvist, *Chem. Phys. Lett.*, 1997, **274**, 196.
76 A. Landau, E. Eliav, Y. Ishikawa and U. Kaldor, *J. Chem. Phys.*, 2004, **121**, 6634–6639.
77 T. J. Lee and P. R. Taylor, *Int. J. Quantum Chem. Symp.*, 1989, **23**, 199.
78 E. Fromager, F. Real, P. Wahlin, U. Wahlgren and H. J. A. Jensen, *J. Chem. Phys.*, 2009, **131**, 054107.
79 R. G. Denning, *J. Phys. Chem.*, 2007, **111**, 4125.
80 K. Tatsumi and R. Hoffmann, *Inorg. Chem.*, 1980, **19**, 2656–2658.
81 J. F. Janak, *Phys. Rev. B*, 1978, **18**, 7165.
82 D. P. Chong, O. V. Gritsenko and E. J. Baerends, *J. Chem. Phys.*, 2002, **117**, 1760.
83 A. Ruzsinszky, J. P. Perdew, G. I. Csonka, O. A. Vydrov and G. E. Scuseria, *J. Chem. Phys.*, 2006, **125**, 194112.
84 P. Mori-Sánchez, A. J. Cohen and W. T. Yang, *J. Chem. Phys.*, 2006, **125**, 201102.
85 S. Kümmel and L. Kronin, *Rev. Mod. Phys.*, 2008, **80**, 30.
86 T. Körzdorfer, S. Kümmel and M. Mundt, *J. Chem. Phys.*, 2008, **129**, 014110.
87 D. J. Tozer, *J. Chem. Phys.*, 2003, **119**, 12697.
88 D. J. Tozer and N. C. Handy, *Phys. Chem. Chem. Phys.*, 2000, **2**, 2117.
89 J. B. Krieger, Y. Li and J. Iafrate, *Phys. Rev. A*, 1992, **45**, 101.
90 A. M. Teale, F. D. Proft and D. J. Tozer, *J. Chem. Phys.*, 2008, **129**, 044110.
91 A. J. Cohen, P. Mori-Sanchez and W. Yang, *J. Chem. Phys.*, 2007, **126**, 191109.
92 B. G. Janesko, T. M. Henderson and G. E. Scuseria, *Phys. Chem. Chem. Phys.*, 2009, **11**, 443–454.
93 T. M. Henderson, A. F. Izmaylov, G. Scalmani and G. E. Scuseria, *J. Chem. Phys.*, 2009, **131**, 044108.
94 J.-W. Song, M. A. Watson, A. Nakata and K. Hirao, *J. Chem. Phys.*, 2008, **129**, 184113.
95 K. Capelle, *J. Braz. Phys. Soc.*, 2006, **36**, 1318.
96 D. Jacquemin, E. A. Perpéte, I. Cioni and C. Adamo, *J. Chem. Theory Comput.*, 2010, **6**, 1532.
97 J. Preat, D. Jacquemin, J.-M. A. V. Wathelet and E. A. Perpéte, *J. Phys. Chem. A*, 2006, **110**, 8144.
98 D. Jacquemin, V. Wathelet, E. A. Perpéte, I. Cioni and C. Adamo, *J. Chem. Theory Comput.*, 2009, **5**, 2420.
99 D. Jacquemin, E. A. Perpte, I. Ciofini, C. Adamo, R. Valero, Y. Zhao and D. G. Truhlar, *J. Chem. Theory Comput.*, 2010, **6**, 2071.
100 M. A. Rohrdanz, K. M. Martins and J. M. Herbert, *J. Chem. Phys.*, 2009, **130**, 054112.
101 M. Silva-Junior, M. Schreiber, S. P. A. Sauer and W. Thiel, *J. Phys. Chem.*, 2008, **129**, 104103.
102 M. Silva-Junior, M. Schreiber, S. Sauer and W. Thiel, *J. Phys. Chem.*, 2010, **133**, 174318.
103 I. Ciofini and C. Adamo, *J. Phys. Chem. A*, 2007, **111**, 5549–5556.

Table 1 Comparison of different xc functionals for UO_2^{2+} (in eV). S-T indicates singlet-triplet splitting, MUE the mean absolute error and Max the maximum absolute error, respectively.

XC/Hamiltonian	$1^3\Phi_g$	$1^1\Phi_g$	S-T	$1^3\Delta_g$	$1^1\Delta_g$	S-T	$1^3\Gamma_g$	$1^1\Gamma_g$	S-T	$1^3\Phi_u$	$1^1\Phi_u$	S-T	$1^3\Delta_u$	$1^1\Delta_u$	S-T	MUE	Max
ZORA/LDA	2.02	2.46	0.44	2.36	3.07	0.71	3.37	3.57	0.20	2.99	3.07	0.08	3.47	3.48	0.01	1.04	1.70
DC/LDA	2.04	2.54	0.50	2.37	3.22	0.85	3.38	3.66	0.28	3.00	3.08	0.08	3.47	3.50	0.03	1.00	1.69
ZORA/PBE(ALDA)	2.01	2.45	0.44	2.40	3.10	0.70	3.38	3.58	0.20	3.04	3.12	0.08	3.57	3.59	0.02	1.00	1.65
DC/PBE(ALDA)	2.03	2.53	0.50	2.41	3.25	0.84	3.38	3.65	0.27	3.04	3.12	0.08	3.55	3.58	0.03	0.97	1.65
DC/PBE	1.73	2.46	0.73	2.05	3.16	1.11	3.20	3.59	0.39	2.99	3.11	0.12	3.51	3.57	0.06	1.09	1.70
ZORA/BLYP(ALDA)	2.01	2.46	0.45	2.43	3.11	0.66	3.31	3.52	0.21	3.00	3.08	0.08	3.55	3.56	0.01	1.02	1.69
DC/BLYP(ALDA)	2.05	2.55	0.50	2.45	3.26	0.81	3.31	3.58	0.27	3.00	3.09	0.09	3.53	3.56	0.03	0.99	1.69
DC/BLYP	1.84	2.45	0.61	2.22	3.13	0.91	3.19	3.50	0.31	2.98	3.08	0.10	3.50	3.55	0.05	1.08	1.71
ZORA/M06-L(ALDA)	2.38	2.84	0.46	2.71	3.46	0.75	3.77	3.97	0.20	3.60	3.68	0.08	4.08	4.08	0.00	0.61	1.09
ZORA/B3LYP(XALDA)	2.30	2.80	0.51	2.51	3.39	0.88	4.01	4.23	0.22	4.22	4.31	0.09	4.57	4.58	0.01	0.34	0.56
DC/B3LYP(XALDA)	2.37	2.92	0.55	2.58	3.59	1.01	4.04	4.31	0.27	4.23	4.33	0.10	4.56	4.61	0.05	0.29	0.53
DC/B3LYP	2.21	2.84	0.63	2.40	3.49	1.08	3.95	4.26	0.31	4.20	4.32	0.12	4.53	4.59	0.06	0.35	0.62
ZORA/PBE0(XALDA)	2.35	2.88	0.53	2.50	3.43	0.94	4.25	4.48	0.23	4.56	4.66	0.10	4.84	4.85	0.01	0.19	0.36
DC/PBE0(XALDA)	2.42	2.99	0.57	2.58	3.63	1.05	4.29	4.57	0.28	4.57	4.68	0.11	4.84	4.89	0.05	0.16	0.28
DC/PBE0	2.15	2.94	0.79	2.24	3.57	1.33	4.15	4.54	0.39	4.53	4.67	0.14	4.79	4.88	0.09	0.22	0.55
ZORA/M06(XALDA)	2.42	2.97	0.54	2.52	3.50	0.98	4.26	4.49	0.23	4.60	4.70	0.10	4.84	4.85	0.01	0.16	0.31
ZORA/M06-2X(XALDA)	2.34	2.94	0.60	2.23	3.35	1.12	4.94	5.21	0.27	5.63	5.74	0.11	5.57	5.62	0.05	0.56	1.00
ZORA/SAOP(ALDA)	3.07	3.51	0.44	3.27	4.00	0.73	4.29	4.48	0.19	4.21	4.29	0.08	4.55	4.56	0.01	0.37	0.79
DC/SAOP(ALDA)	3.01	3.50	0.49	3.24	4.10	0.86	4.33	4.57	0.24	4.22	4.31	0.09	4.59	4.63	0.04	0.35	0.76
DC/CAM-B3LYP(XALDA)	2.56	3.13	0.57	2.71	3.77	1.06	4.41	4.69	0.26	4.70	4.81	0.11	4.93	5.00	0.07	0.15	0.29
DC/CAM-B3LYP	2.43	3.07	0.64	2.56	3.69	1.13	4.36	4.65	0.29	4.69	4.81	0.12	4.91	4.99	0.08	0.15	0.28
ZORA/TDHF	3.01	3.78	0.77	2.40	4.00	1.60	7.12	7.17	0.05	8.82	9.00	0.18	8.15	8.54	0.39	2.19	4.26
CASPT2	2.91	3.40	0.49	2.77	3.88	1.11	4.61	4.83	0.22	4.82	4.85	0.03	4.72	4.64	-0.08	0.16	0.31
CASPT2[1]	2.94	3.47	0.57	2.79	3.90	1.11	4.66	4.86	0.20	4.71	4.74	0.03	4.63	4.55	-0.08	0.16	0.33
IHFSCC	2.70	3.24	0.54	2.48	3.57	1.09	4.57	4.78	0.21	4.69	4.74	0.05	4.76	4.71	-0.05		

[1] Ref. [25]

Table 2 Comparison of different XC functionals for NUO^+ (in eV). S-T indicates singlet-triplet splitting, MUE the mean absolute error and Max the maximum absolute error, respectively.

XC/Hamiltonian	$1^3\Phi$	$1^1\Phi$	S-T	$1^3\Delta$	$1^1\Delta$	S-T	$1^3\Gamma$	$1^1\Gamma$	S-T	$1^3\Pi$	$1^1\Pi$	S-T	$2^3\Phi$	$2^1\Phi$	S-T	MUE	Max
ZORA/LDA	0.77	1.09	0.32	1.34	1.73	0.39	2.00	2.14	0.14	2.61	2.98	0.37	2.61	2.65	0.04	0.80	1.31
DC/LDA	0.86	1.20	0.34	1.40	1.88	0.48	2.08	2.29	0.21	2.67	3.13	0.46	2.64	2.84	0.20	0.69	1.23
ZORA/PBE(ALDA)	0.85	1.17	0.32	1.45	1.86	0.41	2.13	2.27	0.14	2.79	3.16	0.37	2.79	2.82	0.03	0.66	1.18
DC/PBE(ALDA)	0.84	1.20	0.36	1.41	1.92	0.51	2.07	2.29	0.22	2.71	3.10	0.39	2.71	2.88	0.17	0.68	1.24
DC/PBE	0.52	1.15	0.63	1.11	1.87	0.76	1.91	2.24	0.33	2.59	3.07	0.48	2.54	2.82	0.28	0.81	1.40
ZORA/BLYP(ALDA)	0.87	1.19	0.32	1.50	1.90	0.40	2.06	2.21	0.15	2.75	3.12	0.37	2.75	2.78	0.03	0.68	1.25
DC/BLYP(ALDA)	0.87	1.23	0.36	1.47	1.96	0.49	2.01	2.23	0.22	2.66	3.05	0.39	2.66	2.84	0.18	0.69	1.30
DC/BLYP	0.67	1.17	0.50	1.28	1.88	0.60	1.89	2.15	0.26	2.59	3.01	0.42	2.54	2.74	0.20	0.80	1.42
ZORA/M06-L(ALDA)	1.13	1.48	0.35	1.68	2.15	0.47	2.55	2.70	0.15	3.18	3.54	0.36	3.18	3.21	0.03	0.34	0.76
ZORA/B3LYP(XALDA)	1.25	1.68	0.43	1.67	2.29	0.62	2.66	2.82	0.16	3.17	3.54	0.37	3.17	3.22	0.05	0.28	0.65
DC/B3LYP(XALDA)	1.29	1.75	0.46	1.68	2.40	0.72	2.62	2.85	0.23	3.11	3.51	0.40	3.12	3.29	0.17	0.26	0.69
DC/B3LYP	1.13	1.68	0.55	1.52	2.33	0.81	2.56	2.80	0.24	3.07	3.48	0.41	3.03	3.23	0.20	0.31	0.75
ZORA/PBE0(XALDA)	1.31	1.76	0.45	1.65	2.34	0.69	2.87	3.05	0.18	3.32	3.70	0.38	3.32	3.37	0.05	0.18	0.44
DC/PBE0(XALDA)	1.34	1.83	0.49	1.67	2.46	0.79	2.84	3.08	0.24	3.28	3.68	0.40	3.28	3.46	0.18	0.19	0.47
DC/PBE0	1.06	1.78	0.68	1.35	2.41	1.06	2.70	3.05	0.35	3.18	3.66	0.48	3.14	3.42	0.28	0.27	0.61
ZORA/M06(XALDA)	1.33	1.79	0.46	1.64	2.36	0.72	2.92	3.09	0.17	3.35	3.72	0.37	3.35	3.40	0.05	0.16	0.39
ZORA/M06-2X(XALDA)	1.32	1.86	0.54	1.34	2.28	0.94	3.39	3.60	0.21	3.54	3.91	0.37	3.57	3.63	0.06	0.21	0.41
ZORA/SAOP(ALDA)	1.93	2.26	0.33	2.34	2.78	0.44	3.02	3.16	0.14	3.50	3.84	0.34	3.50	3.54	0.04	0.31	0.78
DC/SAOP(ALDA)	1.84	2.21	0.37	2.28	2.82	0.54	2.96	3.16	0.20	3.47	3.83	0.36	3.47	3.63	0.16	0.30	0.72
DC/CAM-B3LYP(XALDA)	1.50	1.99	0.49	1.83	2.63	0.80	2.91	3.16	0.25	3.35	3.76	0.41	3.35	3.53	0.18	0.18	0.40
DC/CAM-B3LYP	1.37	1.94	0.57	1.69	2.56	0.87	2.85	3.12	0.27	3.31	3.73	0.42	3.28	3.48	0.20	0.19	0.46
ZORA/TDHF	2.05	2.79	0.74	4.73	5.15	0.42	5.51	5.76	0.25	6.09	6.33	0.24	5.93	6.15	0.22	2.26	3.17
CASPT2	1.88	2.23	0.35	1.84	2.42	0.58		3.19			3.35					0.06	0.29
CASPT2(12,15)	1.89	2.32	0.43	1.90	2.55	0.65	3.18	3.26	0.08	3.20	3.39	0.19				0.06	0.34
IHFSCC	1.59	2.06	0.47	1.56	2.37	0.81	3.31	3.45	0.14	3.34	3.50	0.16	3.36	3.38	0.02		

Table 3 Comparison of different XC functionals for NUN (in eV). S-T indicates singlet-triplet splitting, MUE the mean absolute error and Max the maximum absolute error, respectively.

XC/Hamiltonian	$1^3\Phi_g$	$1^1\Phi_g$	S-T	$1^3\Delta_g$	$1^1\Delta_g$	S-T	$1^3\Phi_u$	$1\,^1\Phi_u$	S-T	$1^3\Gamma_g$	$1^1\Gamma_g$	S-T	$1^3\Sigma_u$	$1^1\Sigma_u$	S-T	MUE	Max
ZORA/LDA	1.07	1.51	0.44	1.64	2.24	0.58	1.88	1.97	0.09	2.26	2.47	0.21	2.34	2.60	0.26	0.78	1.55
DC/LDA	1.13	1.63	0.50	1.67	2.41	0.74	1.95	2.06	0.11	2.32	2.60	0.28	2.21	2.48	0.27	0.74	1.46
ZORA/PBE(ALDA)	1.05	1.49	0.44	1.68	2.26	0.58	1.90	2.00	0.10	2.28	2.49	0.21	2.35	2.60	0.25	0.77	1.52
DC/PBE(ALDA)	1.12	1.62	0.50	1.70	2.43	0.73	1.96	2.07	0.11	2.32	2.60	0.28	2.23	2.49	0.26	0.74	1.45
DC/PBE	0.72	1.54	0.82	1.31	2.34	1.03	1.89	2.05	0.16	2.13	2.54	0.41	2.14	2.47	0.33	0.83	1.49
ZORA/BLYP(ALDA)	1.07	1.51	0.44	1.73	2.28	0.65	1.92	2.01	0.09	2.22	2.43	0.21	2.24	2.51	0.27	0.80	1.51
DC/BLYP(ALDA)	1.16	1.66	0.50	1.76	2.44	0.68	1.98	2.09	0.11	2.27	2.54	0.27	2.14	2.41	0.27	0.76	1.43
DC/BLYP	0.90	1.55	0.65	1.53	2.32	0.79	1.94	2.08	0.14	2.13	2.46	0.33	2.10	2.40	0.30	0.82	1.44
ZORA/M06-L(ALDA)	1.32	1.77	0.45	1.91	2.55	0.64	2.20	2.30	0.10	2.63	2.83	0.20	3.13	3.31	0.18	0.52	1.22
ZORA/B3LYP(XALDA)	1.29	1.79	0.50	1.74	2.53	0.79	2.92	3.04	0.12	2.77	3.00	0.23	2.62	2.93	0.31	0.34	0.60
DC/B3LYP(XALDA)	1.40	1.95	0.55	1.81	2.74	0.93	2.98	3.11	0.13	2.84	3.13	0.29	2.56	2.87	0.31	0.31	0.53
DC/B3LYP	1.21	1.87	0.66	1.62	2.64	1.02	2.95	3.10	0.15	2.74	3.07	0.33	2.53	2.86	0.33	0.33	0.63
ZORA/PBE0(XALDA)	1.32	1.84	0.52	1.69	2.55	0.86	3.18	3.30	0.12	2.97	3.21	0.24	2.87	3.17	0.30	0.19	0.40
DC/PBE0(XALDA)	1.42	1.99	0.57	1.77	2.76	0.99	3.23	3.37	0.14	3.05	3.35	0.30	2.79	3.08	0.29	0.16	0.32
DC/PBE0	1.09	1.94	0.85	1.38	2.70	1.32	3.16	3.36	0.20	2.92	3.31	0.39	2.69	3.06	0.37	0.21	0.45
ZORA/M06(XALDA)	1.34	1.88	0.54	1.70	2.59	0.89	3.16	3.29	0.13	2.98	3.21	0.23	2.97	3.26	0.29	0.20	0.39
ZORA/M06-2X(XALDA)	1.26	1.86	0.60	1.30	2.40	1.10	3.97	4.12	0.15	3.49	3.76	0.27	2.87	3.32	0.45	0.26	0.60
ZORA/SAOP(ALDA)	2.03	2.47	0.44	2.50	3.06	0.56	2.89	2.99	0.10	3.04	3.23	0.19	2.61	2.86	0.25	0.47	1.02
DC/SAOP(ALDA)	1.98	2.47	0.49	2.46	3.18	0.72	2.93	3.04	0.11	3.09	3.35	0.26	2.45	2.71	0.26	0.48	0.98
DC/CAM-B3LYP(XALDA)	1.75	2.14	0.39	1.91	2.91	1.00	3.43	3.57	0.14	3.21	3.48	0.27	2.82	3.16	0.34	0.19	0.43
DC/CAM-B3LYP	1.65	2.08	0.43	1.75	2.83	1.08	3.41	3.57	0.16	3.09	3.42	0.33	2.83	3.18	0.35	0.13	0.28
ZORA/TDHF	1.88	2.66	0.78	1.37	2.98	1.61	6.79	6.98	0.19	5.53	5.84	0.31	3.87	4.54	0.67	1.52	3.46
CASPT2	1.80	2.30	0.50	1.77	2.66	0.89	3.23	3.29	0.06	3.04	3.51	0.47	2.62	2.85	0.23	0.22	0.33
IHFSCC	1.51	2.06	0.55	1.48	2.56	0.88	3.38	3.52	0.14	3.37	3.58	0.21	2.87	3.14	0.27		

Table 4 CASPT2 Mulliken charges for the ground and excited states of UO_2^{2+}, NUO+ and NUN.

	UO_2^{2+}		NUO+				NUN		
State	U	O	State	U	N	O	State	U	N
$X^1\Sigma_g^+$	2.41	-0.21	$X^1\Sigma$	1.72	-0.39	-0.33	$X^1\Sigma_g^+$	0.77	-0.39
$^1\Phi_g$	2.36	-0.18	$^1\Phi$	1.70	-0.57	-0.12	$^1\Phi_g$	0.78	-0.39
$^3\Phi_g$	2.36	-0.18	$^3\Phi$	1.71	-0.57	-0.14	$^3\Phi_g$	0.76	-0.38
$^1\Delta_g$	2.35	-0.17	$^1\Delta$	1.73	-0.55	-0.19	$^1\Delta_g$	0.76	-0.38
$^3\Delta_g$	2.37	-0.18	$^3\Delta$	1.70	-0.57	-0.13	$^3\Delta_g$	0.79	-0.39
$^1\Gamma_g$	2.25	-0.13	$^1\Gamma$	1.70	-0.57	-0.12	$^1\Phi_u$	0.74	-0.37
$^3\Gamma_g$	2.26	-0.13	$^3\Gamma$	–	–	–	$^3\Phi_u$	0.72	-0.36
$^1\Phi_u$	2.25	-0.13	$^1\Pi$	1.74	-0.57	-0.17	$^1\Gamma_g$	0.78	-0.39
$^3\Phi_u$	2.26	-0.13	$^3\Pi$	–	–	–	$^3\Gamma_g$	0.79	-0.40
$^1\Delta_u$	2.26	-0.13	$2^1\Phi$	–	–	–	$^1\Sigma_u$	0.64	-0.33
$^3\Delta_u$	2.26	-0.13	$2^3\Phi$	–	–	–	$^3\Sigma_u$	0.64	-0.32

Table 5 Comparison of DFT and IHFSCC for the first three ionization potentials (IPs) for UO_2^{2+}, NUO+ and NUN (in eV). As these ionized states in the IHFSCC are dominated by contributions from a single orbital and the DFT values are approximated by the negative of the orbital energies, we identify the IPs with the respective orbitals (which range from HOMO-2 to HOMO for DFT). ZORA and DC are Zero Order Regular Approximated and Dirac-Coulomb Hamiltonians, respectively.

		NUN			NUO^+			UO_2^{2+}		
		π_u	σ_g	σ_u	σ(U-O)	π	σ(U-N)	π_u	σ_g	σ_u
LDA	ZORA	6.58	6.08	5.50	14.57	13.78	12.59	23.45	22.95	22.22
	DC	6.53	6.05	5.46	14.51	13.63	12.47	23.39	22.87	22.16
PBE	ZORA	6.32	5.84	5.22	14.33	13.52	12.32	23.19	22.74	21.94
	DC	6.29	5.82	5.21	14.28	13.38	12.23	23.12	22.66	21.90
BLYP	ZORA	6.18	5.76	5.15	14.22	13.36	12.24	23.02	22.59	21.84
	DC	6.16	5.77	5.17	14.18	13.22	12.16	22.95	22.52	21.81
M06-L	ZORA	6.25	5.72	5.07	14.40	13.53	12.12	23.19	22.91	21.93
B3LYP	ZORA	7.26	6.85	6.50	15.63	14.45	13.59	24.36	24.03	23.39
	DC	7.24	6.83	6.50	15.61	14.40	13.50	24.32	23.98	23.38
PBE0	ZORA	7.57	6.85	6.50	16.01	14.90	13.92	24.76	24.45	23.78
	DC	7.54	7.08	6.79	15.98	14.76	13.82	24.72	24.39	23.76
M06	ZORA	7.56	7.10	6.97	16.07	14.92	13.99	24.73	24.46	23.97
M06-2X	ZORA	8.86	8.30	8.58	17.66	16.24	15.45	26.27	25.90	25.64
SAOP	ZORA	10.16	9.92	9.28	18.73	17.69	16.69	27.82	27.64	26.72
	DC	10.08	9.83	9.10	18.62	17.52	16.49	27.76	27.55	26.57
CAM-B3LYP	DC	9.02	8.48	8.44	17.49	16.22	15.37	26.23	25.78	25.40
IHFSCC	DC	10.15	9.45	9.43	18.66	17.76	16.74	27.76	27.15	27.08

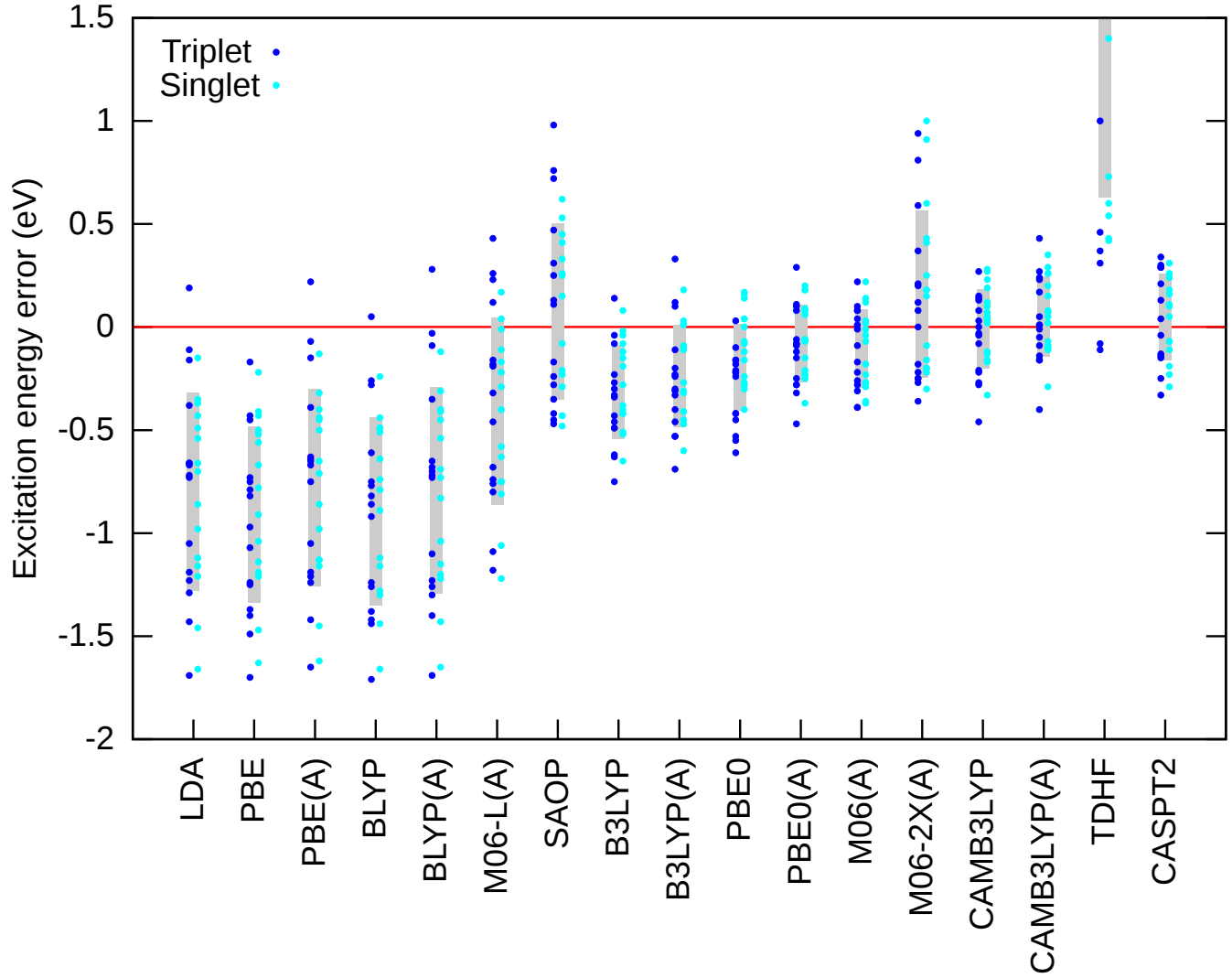

Fig. 1 Errors with respect to IHFSCC for all excitations and all molecules. The gray boxes enclose a range of one sample standard deviation above and below the average error. Dots show individual errors for each excitation energy. The two highest (DFT) states for NUO+ has been left out of the analysis. (ALDA) – evaluated using the ALDA approximation.

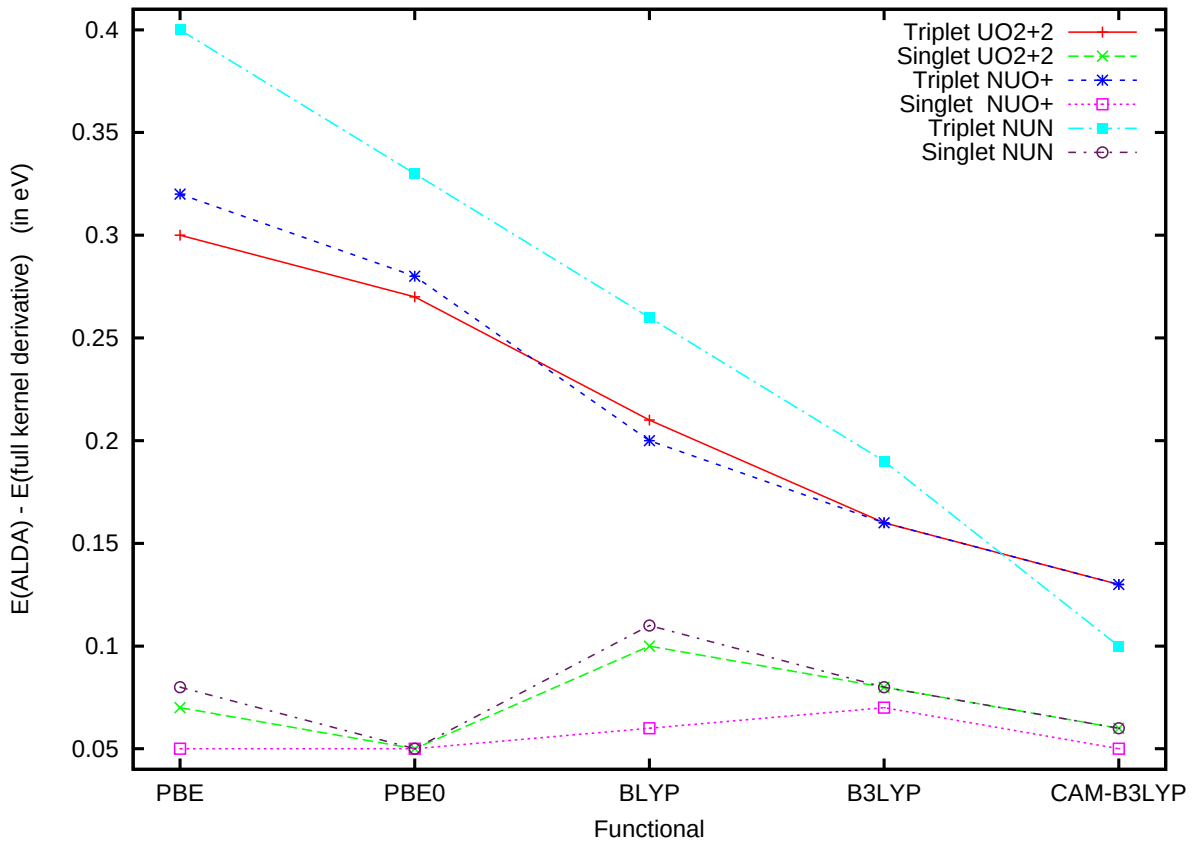

Fig. 2 Errors for the first singlet and triplet Φ states due to the ALDA approximation for the PBE, PBE0, BLYP, B3LYP and CAM-B3LYP functionals.